A Search for Lunar Radio Čerenkov Emission from High-energy Neutrinos

T. H. Hankins[1], R. D. Ekers[2], and J. D. O'Sullivan[3]

[1]*New Mexico Institute of Mining and Technology, Socorro, NM 87801*
[2]*Australia National Telescope Facility, Epping, NSW 2121 Australia*
[3]*News Limited, Surrey Hills, NSW, 2010, Australia*

Abstract.
We describe a 10-h search for the radio signature of high-energy neutrinos interacting with the near surface of the Moon. The upper limit of the amplitude of the 1-ns duration expected pulses in the 1.5-GHz frequency range, dispersed by one passage through the Earth's ionosphere, is about 400 Jy. We describe here some details of the observations and analysis.

INTRODUCTION

The search for the highest energy particles in the Universe requires enormous detector volumes, partly because their flux is extremely low, and because, in the case of neutrinos, their interaction cross-sections are very small. To increase the detection probability, then, large volumes of matter are required. To this end detectors have been placed in the clear, deep ocean, and in the South polar ice cap to detect Čerenkov radiation from the particle cascade resulting from a neutrino interaction in water. Dagkesamansky and Zheleznykh [1] suggested that if a neutrino has an interaction in the near surface of the Moon, then the radio-frequency Čerenkov emission could escape through ≈10-m of lunar rock, and might be detectable by a sensitive radio telescope on the Earth. The Moon offers a surface area of $10^7\,\mathrm{km}^2$ and a volume of $10^{14}\,\mathrm{m}^3$, which is more than 1000 times larger than the Antarctic ice detector volume.

Our experience with high-time resolution pulsar studies and the removal of dispersion effects from pulsar signals due to propagation through the interstellar medium led us to design an experiment to test the hypothesis of Dagkesamansky and Zheleznykh, that $E > 10^{20}\,\mathrm{eV}$ neutrino interaction cascades in the near 10-m of the Moon produce 1-ns radio pulses from Čerenkov emission. Our strategy was to look for short, dispersed pulses from the Moon, using existing equipment wherever possible. We have described our results in a previous paper [2]. Here we expand on some of the observational details of our experiment.

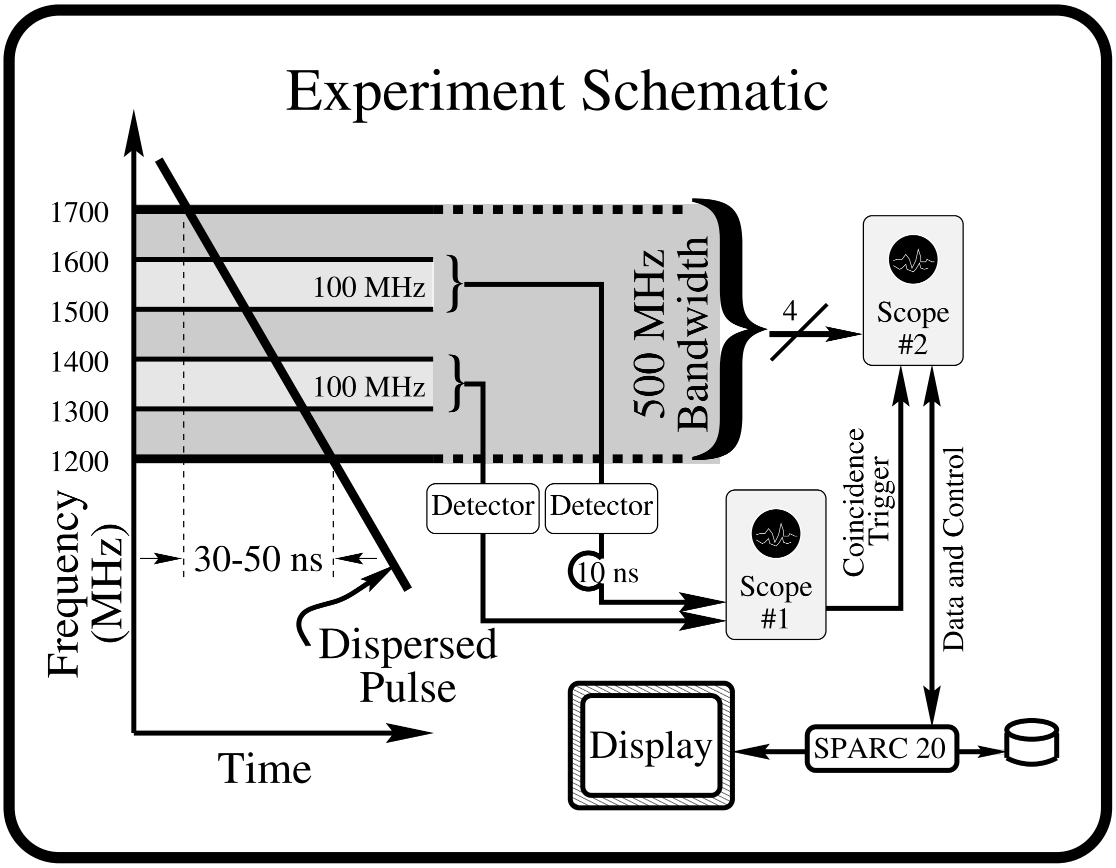

FIGURE 1. Schematic diagram of the data acquisition system.

EXPERIMENT

We used the 64-m telescope at Parkes, NSW, Australia, which had recently been outfitted with a wide-band, dual-polarization receiver constructed for the SETI program. The receiver covers 1.2 to 1.9 GHz; we used a relatively interference-free bandwidth of 500 MHz centered on 1425 MHz to maximize the bandwidth of the signals and to allow 2-ns time resolution of the signals. When pointed at the Moon the receiver's noise temperature is dominated by the 250 K thermal noise from the Moon, yielding a limiting sensitivity (one standard deviation fluctuation of the radiometer square-law detector output with time-bandwidth product equal to 1) of about 450 Jy. The telescope beam-width is 13 arcmin (FWHM), so when the telescope was pointed at the Moon's center we had somewhat reduced sensitivity near the limb.

A schematic diagram of the experimental setup is shown in Figure 1. The received signal was amplified and mixed to a center frequency of 475 MHz; in Figure 1 the signal is shown spanning 1200–1700 MHz. The full 500 MHz from each of two polarizations was fed to two sets of quadrature mixers. These mixers split each polarization into two parts which were then multiplied by $\cos(2\pi f_{\rm m}t)$ and $\sin(2\pi f_{\rm m}t)$ respectively, where $f_{\rm m} = 475\,\mathrm{MHz}$. The mixer outputs are then low-pass filtered to form what we call the in-phase and quadrature parts of each polarization. The mixer oscillator signals at 475 MHz and the mixer output pairs were carefully checked for orthogonality. The four resulting 0 to 250 MHz signals were simultaneously sampled by the LeCroy 9354L oscilloscope.

Triggering

To form trigger channels the full bandwidth was also passed to two 100-MHz wide filters whose center frequencies were separated by 200 MHz. The filter outputs were square-law detected using special detectors with output rise-times $<10\,\mathrm{ns}$. We expected the dispersed Čerenkov pulse to be smeared by dispersion across the bandpass by 30 to 50 ns by one pass through the ionosphere. It should therefore reach the upper frequency detector channel 10 to 20 ns before the lower detector channel. By inserting an extra (10-foot) length of coax cable we delayed the upper-frequency channel signal relative to the lower-frequency channel by the expected dispersion delay. We selected the LeCroy 9354L trigger mode which requires two-channel coincidence *and* a pulse width within the (settable) limits 7.5 to 20 ns. The coincidence trigger allows us to minimize the false-alarm probability from random radiometer noise and terrestrial interference. Figure 2 shows a typical detection event. When coincidence was detected, the oscilloscope *output* a trigger signal that was used to "grab" the wide-band, quadrature signals sampled by a separate LeCroy 9354L oscilloscope. The second oscilloscope was sampling continuously at 500 MS/s to a circular memory; it uses the coincidence trigger as a "stop" command, so that data before and after the trigger can be stored. We saved $1\,\mu$s data (500 2-ns samples per channel) centered on the trigger epoch. The data from the second oscilloscope were then immediately transferred to a Sun Sparc 20 computer, where they were archived and analyzed at a number of trial dispersion values and displayed in quasi-real time.

Detection Criteria

To be considered a real lunar event, we required three criteria to be met.

1. A dedispersed event must be coincident with the trigger time; otherwise it must be considered a fortuitous realignment of noise by the dedispersion filtering process.
2. Since Čerenkov radiation is linearly polarized, and our receiver channels are orthogonally circularly polarized, an event must appear simultaneously in both dedispersed channels.
3. The dedispersion reconstruction must produce an impulse with the correct dispersion value.

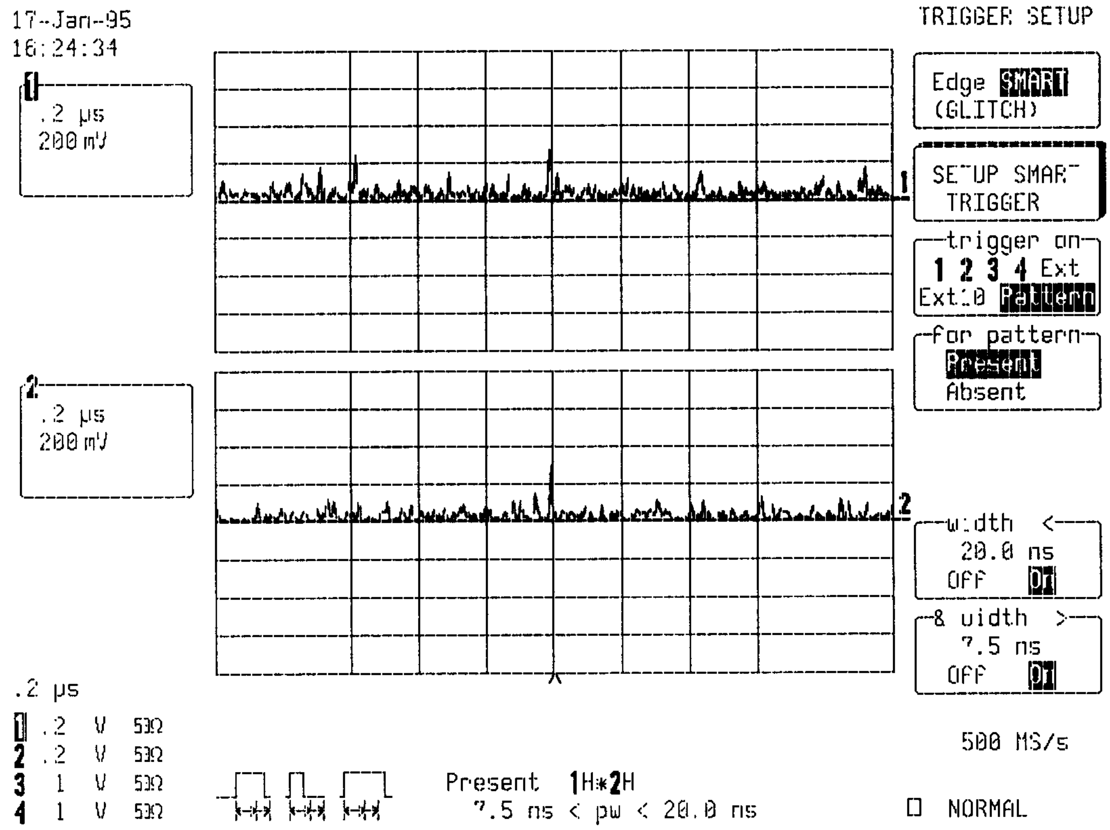

FIGURE 2. Trigger oscilloscope display of a typical event. The trigger point is set to the center of the traces as indicated by the caret symbol below the lower trace. The upper trace shows the square-law detected signal in the 1300–1400 MHz band, and the lower trace shows the (delayed) signal from the 1500–1600 MHz band. The total trace time shown is $2\,\mu$s, and the sample rate is 500 MS/s. The coincidence trigger threshold levels were set to 8 times the *rms* detected signal level.

Ionospheric Dispersion

Since our receiver passband is narrow relative to its center frequency, we may represent the electric field, s(t), of the lunar radio event in narrow-band signal or complex-envelope notation. (The frequency limits set by the receiver bandwidth are implicit in the following discussion. To keep the presentation simple, the effects of quadrature mixing the signal to a center frequency of zero are omitted. See [3] for details.)

$$s_{\text{emitted}}(t) = \Re\left\{a(t)e^{i\omega t}\right\},$$

where $a(t)$ is the narrow-band, complex envelope of the signal, and we assume that the bandwidth of $s(t)$ is centered around ω. Propagation through ionosphere is equivalent to passing the signal through a filter:

$$s_{\text{received}}(t) = s_{\text{emitted}}(t) * h(t)$$

where $h(t) =$ impulse response of the ionosphere and $*$ denotes convolution. We can write this in the frequency domain using $S(\omega) \equiv$ Fourier transform $\{s(t)\}$. Then

$$S_{\text{received}}(\omega) = S_{\text{emitted}}(\omega) \cdot H(\omega).$$

$H(\omega) = e^{ik(\omega)z}$ is (formally) the Transfer Function of the ionosphere of thickness z. But $k(\omega) = n\omega/c$ and $n =$ refractive index of the ionosphere. For a cold plasma $n^2 = 1 - \omega_{\text{p}}^2/\omega^2$, where $\omega_{\text{p}} = \sqrt{N_{\text{e}}e/m_{\text{e}}\epsilon_0}$ is the plasma frequency of the ionosphere. N_{e}, e, and m_{e} are the electron density, charge, and mass. Then

$$H(\omega) = \exp\left(i\left(1 - \frac{N_{\text{e}}e}{m_{\text{e}}\epsilon_0}\right)\frac{\omega}{c} \cdot z\right)$$

The factor $N_{\text{e}}z$ is usually written as dispersion measure or *slant total electron content* of the propagation path, $DM = STEC = \int_z N_{\text{e}}\, dz$. Since $H(\omega)$ is frequency dependent, lower radio frequencies have a slower group velocity and hence arrive at Earth later than high frequencies. So the lunar impulsive events received in a finite bandwidth are smeared out by the time it takes the signal to "sweep" from the higher to lower frequency edge of the receiver passband.

The dispersed signal then provides a unique signature for discriminating between events of lunar (dispersed by passage through the ionosphere) and terrestrial origin.

Dispersion Removal Processing

The dispersion distortion suffered by the lunar radio events is linear and can easily be removed by inverse filtering. To recover the signals as they were emitted we need only to multiply the Fourier transform of the received signal by $H^{-1}(\omega) = e^{-ik(\omega)z}$:

$$\begin{aligned} S_{\text{received}}(\omega)H^{-1}(\omega) &= S_{\text{emitted}}(\omega) \cdot H(\omega)H^{-1}(\omega) \\ &= S_{\text{emitted}}(\omega) \overset{\text{FT}}{\Longleftrightarrow} s_{\text{emitted}}(t) \end{aligned}$$

In Figure 3 is shown the result of a simulation of the dedispersion process. A noise-free dispersed pulse with a STEC of 0.56×10^{14} el/cm^3 has been dedispersed using inverse filters with 100 trial values of STEC from 0 to $2(0.56 \times 10^{14})$ el/cm^3. The time axis is plotted so that the nominal arrival time of the dispersed pulse at the center of the receiver passband is at time 0.0. The magnitude of the dispersed pulse with zero dispersion removed appears as a low rectangle centered at $t = 0.0$. Each subsequent trace has been shifted one sample to the right for clarity. The effectiveness of the dedispersion processing gain is readily apparent. When the filter

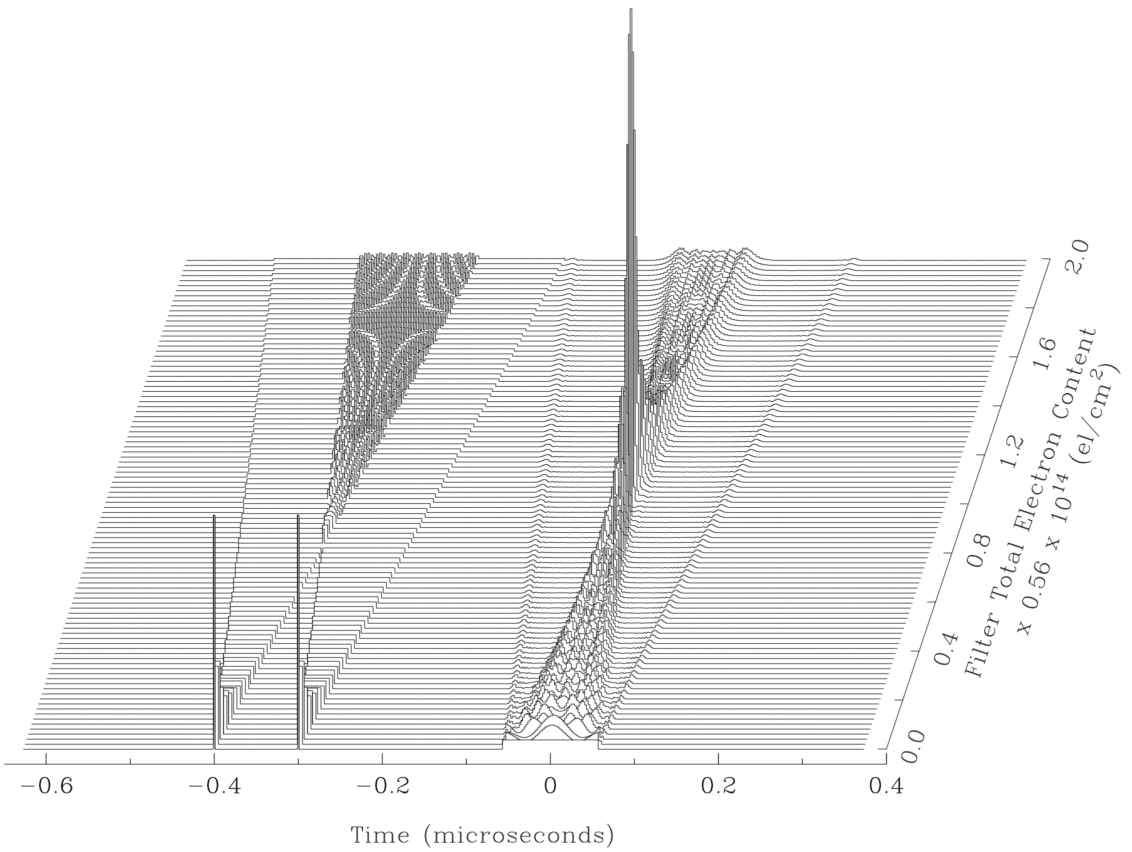

FIGURE 3. Simulation of dispersed and local interfering pulses. The simulated lunar event was dispersed by passage through an ionosphere whose slant total electron content was $0.56 \times 10^{14}\,\mathrm{el/cm^3}$.

dispersion matches the test signal dispersion the original impulse is reconstructed and nearly all of its power appears in a single time sample. The *dispersed* pulse duration is τ_d, which corresponds to $N_\mathrm{d} = \tau_\mathrm{d}\Delta\nu$ complex time samples when the receiver bandpass $\Delta\nu$ is properly sampled at the Nyquist rate. The processing gain, g_d, which we define as the ratio of the dedispersed pulse amplitude to the average value of the dispersed signal while it is in the receiver passband, is $g_\mathrm{d} \approx N_\mathrm{d}$.

When noise is present, and in particular, impulsive terrestrial interference, the effective processing gain is somewhat reduced. Since the dispersion removal filter is an "all-pass" filter, none of the interfering frequency components in the passband are rejected; they are instead rearranged in time. In Figure 3 we show the effect of two noise-free impulses arriving at $t = -0.4$ and $-0.3\,\mu$s. Since they are dispersed by the inverse filter rather than passage through the ionosphere, they become spread out in time as they are filtered with larger STEC values. When several local interference pulses arrive nearby in time, as shown in Figure 3, their filter responses may overlap and superpose imitating a real lunar event. Therefore we scrutinized each captured event to be sure that superposition of local events did not masquerade as lunar events.

For the simulation calculations in Figure 3 a perfectly rectangular receiver pass-band was used. This causes the sidelobes or edge effects seen in the figure. Simulations with Hanning or Hamming weighting of the spectra show considerably reduced edge effects at a cost of about a factor of 2 in processing gain. The actual receiver pass-bands were established by ordinary analog Butterworth filters which do not have sharp band-edge cutoffs, and hence do not produce edge effects as pronounced as in the simulation. Nonetheless, we analyzed all of the data with and without Hanning spectral weighting.

To maximize the processing gain, then, we should use the lowest practical frequency (assuming that the event spectrum is flat), the widest possible bandwidth and the largest STEC. For our experiment the receiver center frequency was chosen to coincide with the radioastronomy protected $\lambda 21$ (1.4 GHz) band, and the bandwidth was determined by the maximum sampling rate available. Despite the fact that the ionospheric STEC is 3–5 times larger in the daytime than at night, we chose night time to avoid interference. Our expected processing gain was therefore about $g_\mathrm{d} \approx 10$. We used values of STEC more appropriate for the daytime ionosphere in the simulation of Figure 3, where $g_\mathrm{d} \approx 50$. Note that observing at low elevation angles can also increase the actual STEC, and thereby increase the ionospheric signature on lunar events.

For our quasi-realtime display and subsequent re-analysis we plotted the dedispersed signals in a format similar to Figure 4, but with fewer (20) trial values of STEC, and we plotted the two polarizations in different colors and with opposite signs.

In Figure 4 we show a typical event processed with our experimental parameters. The STEC used for the dedispersion processing was obtained from the Australian Ionospheric Prediction Service for the epochs of our observations. The central impulse meets criterion 1, but it does not appear in both polarizations. Since its width does not change with filter STEC, it must be an impulse with a narrower bandwidth than our receiver, and therefore does not meet criterion 3. Furthermore, we see a second weak event about 180 ns after the trigger event. We found this to be typical of the signature of local automobile ignition noise. Therefore we reject this event.

We recorded about 700 events in 10 hours over the course of three nights. At least 30% of these were easily attributable to ignition noise (when ignition interference was clearly present, we disabled the triggering system). We set the detector thresholds at a level that should have produced several hundred random triggers; careful inspection of the data off-line did not reveal any events which we consider significant.

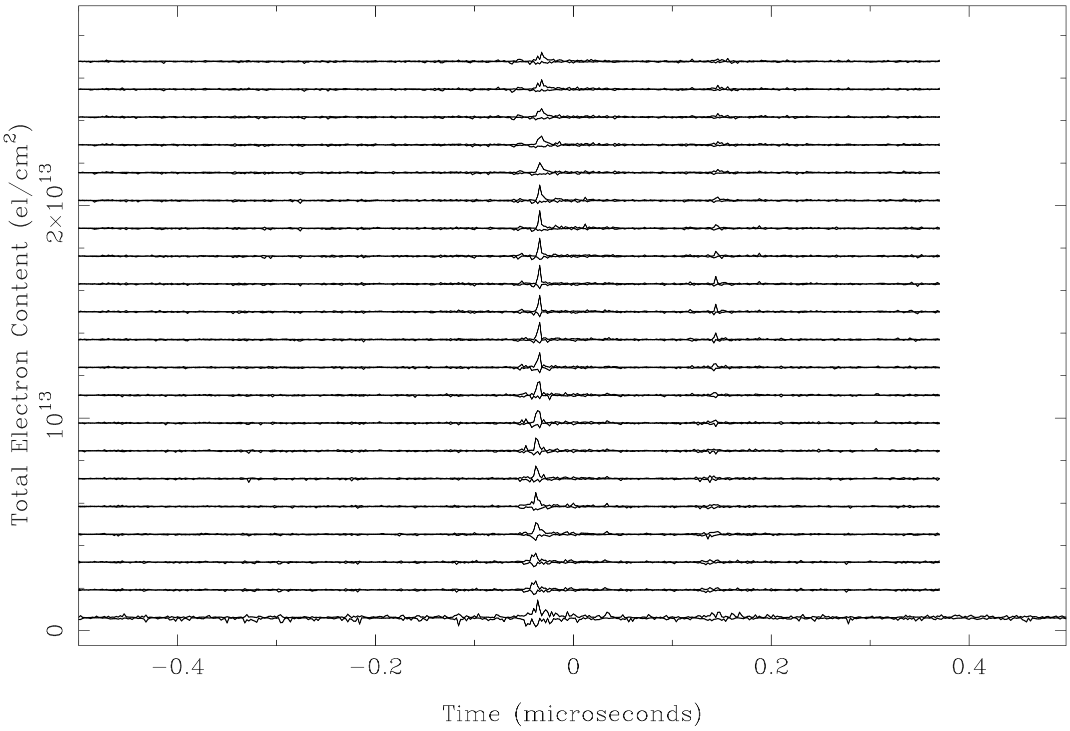

FIGURE 4. A typical event is shown, dedispersed using 20 trial values of STEC from 0 to 2 times the predicted value of 0.14×10^{14} el/cm^3, and plotted with the full 2-ns time resolution. The unfiltered, but square-law detected data are shown as the bottom trace. One circular polarization is plotted upwards, the other downwards.

CONCLUSIONS

Radio detection of lunar Čerenkov events is feasible, but it requires careful rejection of impulsive terrestrial interference. There are several ways to improve the "false-alarm" response of our experiment. Foremost is to use spatial receiver diversity and insist upon temporal coincidence of events that could only come from the Moon's direction. Since the sample rates required to capture the expected pulses are so high, it is only practical to arrange for coincidence tests in real time. Then the communications link bandwidth between spaced receivers must be wide to preserve the time resolution. We feel that the dispersion signature of the ionosphere is essential for identifying any received pulses as extra-terrestrial. Our two-channel coincidence triggering scheme was crude, and could certainly be improved by the addition of more detector/delay triggering channels on both polarizations. In principle one could tailor an antenna or array beam so that it would "illuminate" only the limb of the Moon where events are more likely, but this would require new techniques. Finally, frequency diversity could be employed to take additional advantage of the ionospheric dispersion delay. However, finding adequately wide, interference-free radio spectrum below 1 GHz would be difficult anywhere this side of the Moon!

ACKNOWLEDGMENTS

We thank Mal Sinclair and George Graves for building the fast detectors. We would like to acknowledge Mark Lotter, Scientific Devices, Sydney, Australia, for the generous loan of the second LeCroy 9354L oscilloscope, the National Science Foundation for support through grants AST-9315285 and AST-9618408, and the Australia Telescope National Facility for sabbatical year support of THH. The Parkes Radio Telescope is operated as part of the ATNF, a division of CSIRO. We thank Project Phoenix of SETI Institute for use of the wide-band receiver, and Jiping Wu, Australian Ionospheric Prediction Service for STEC. THH thanks Peter Gorham and David Saltzberg for their kind invitation to RADHEP-2000.

REFERENCES

1. Dagkesamansky R. D., Zheleznykh I. M., 1992, in Nagano, M. and Takahara, F., eds, Astrophysical Aspects of the Most Energetic Cosmic Rays, 1992, World Scientific, Singapore, p. 373
2. Hankins T. H., Ekers R. D., and O'Sullivan J. D. 1996, MNRAS, 283, 1027
3. Hankins T. H., Rickett B. J., 1975, Meth. Comp. Phys., 14, 55